ACS APPLIED MATERIALS & INTERFACES

Research Article

www.acsami.org

# Exploring the Different Photocatalytic Performance for Dye Degradations over Hexagonal $ZnIn_2S_4$ Microspheres and Cubic $ZnIn_2S_4$ Nanoparticles

Yongjuan Chen,[†] Renkun Huang,[†] Daqin Chen,[‡] Yuansheng Wang,[‡] Wenjun Liu,[†] Xiaona Li,[†] and Zhaohui Li*,[†]

[†]Research Institute of Photocatalysis, State Key Laboratory Breeding Base of Photocatalysis, Fuzhou University, Fuzhou 350002, People's Republic of China

[‡]State Key Laboratory of Structural Chemistry, Fujian Institute of Research on the Structure of Matter, Chinese Academy of Sciences, Fuzhou, 350002, People's Republic of China

Supporting Information

**ABSTRACT:** Different pathways for the degradation of rhodamine (RhB) as well as different activity order for the degradation of RhB and methyl orange (MO) were observed over hexagonal $ZnIn_2S_4$ microspheres and cubic $ZnIn_2S_4$ nanoparticles. A detailed study of the physicochemical and surface properties of these two $ZnIn_2S_4$ polymorphs has been carried out to elucidate these phenomena. The results reveal that hexagonal $ZnIn_2S_4$ microspheres are composed of nanolamella petals growing in the *ab* plane, i.e., the negative (0001) S plane. This negative (0001) S plane not only is favorable for the adsorption of the cationic dye RhB via —$N(Et)_2$ groups but also can accumulate the photogenerated holes. These make the hole-directed photocatalytic de-ethylation of RhB more expedient over hexagonal $ZnIn_2S_4$ microspheres. This negative (0001) S plane of hexagonal $ZnIn_2S_4$ microspheres also shows promoting effect for the degradation of cationic dye like MB, but not for the degradation of anionic dye like MO. Our result provides some new insights in how the surface facet can take effect on influencing the performance of a photocatalyst and why different polymorphs can exhibit different photocatalytic performance.

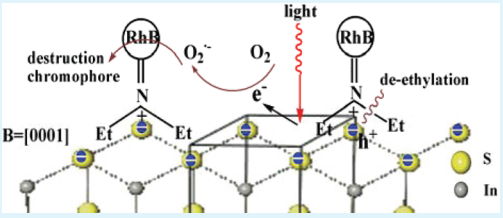


**KEYWORDS:** *$ZnIn_2S_4$, photocatalysis, dye, crystal facet, adsorption*

## 1. INTRODUCTION

People use dyes all their lives. Dyes enrich our life but also destroy our life. About 15% of the total world production of dyes is lost during the dyeing process and the pollution from the dyes containing wastewater has long been a worldwide problem. Several technological systems have already been used to treat the dyes containing wastewater. Among them, heterogeneous photocatalytic oxidation (PCO) is considered to be a green technology for the decomposition of soluble dyes in wastewater because it can use the solar energy.[1−3] However, the commonly used photocatalyst $TiO_2$ has a large band gap, which restricts its practical applications. Therefore, during the past decade, tremendous effort has been devoted to the development of new photocatalysts and a series of impressive visible-light-responsive photocatalysts have been reported.[4−10]

$ZnIn_2S_4$ is a ternary chalcogenide with two distinct polymorphs based on cubic and hexagonal lattices.[11] Both $ZnIn_2S_4$ polymorphs have a variety of applications. For example, hexagonal $ZnIn_2S_4$ has been reported to exhibit photoluminescence[12] and photoconductivity,[13] whereas cubic $ZnIn_2S_4$ has been found to exhibit thermoelectricity.[14] Recently, the photocatalytic activities of both $ZnIn_2S_4$ polymorphs for water splitting as well as organic dyes degradations under visible light irradiations have also been revealed.[15−19] Our recent study reported that cubic $ZnIn_2S_4$ nanoparticles and hexagonal $ZnIn_2S_4$ microspheres can be controllably synthesized and cubic $ZnIn_2S_4$ nanoparticles exhibits a higher photocatalytic activity for the degradation of methyl orange (MO) than the hexagonal one.[20] However, when we used these two $ZnIn_2S_4$ polymorphs in the photocatalytic degradation of rhodamine B (RhB), a cationic dye, an opposite result was obtained. Hexagonal $ZnIn_2S_4$ microspheres exhibit higher photocatalytic activity for the degradation of RhB as compared to cubic $ZnIn_2S_4$ nanoparticles. In addition to this, two $ZnIn_2S_4$ polymorphs show different pathways in the degradation of RhB.

The observation of a higher activity for RhB degradation and a lower activity for MO degradation over hexagonal $ZnIn_2S_4$ microspheres as compared to cubic $ZnIn_2S_4$ nanoparticles is interesting because selectivity in the photocatalytic reactions is seldom reported previously. Usually, the performance of a photocatalyst is influenced by its crystal structure, electronic structure and physicochemical properties like surface area as well as its surface structure since photocatalytic reactions primarily take place on the surface. Because of the anisotropy of the crystal, different crystal facets usually exhibit different properties.[21,22] To elucidate the different photocatalytic

Received: February 16, 2012
Accepted: April 6, 2012
Published: April 12, 2012

  

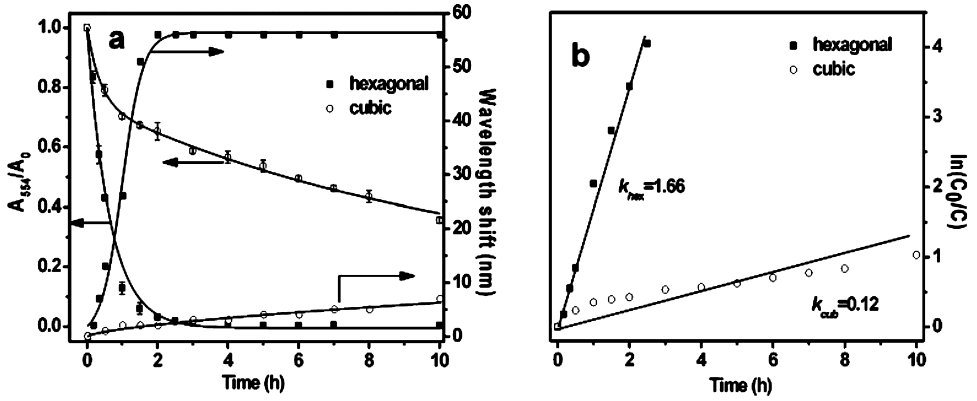


**Figure 1.** (a) Maximum absorbance (554 nm) of RhB changes and wavelength shifts of the major absorption band with irradiation time, and (b) pseudofirst-order plots comparing photocatalytic of degradation RhB, where $k_{cub}$ and $k_{hex}$ are the first-order rate constant of cubic and hexagonal $ZnIn_2S_4$, respectively.

performances in the degradations of different dyes over these two $ZnIn_2S_4$ polymorphs, a detailed study on the physicochemical and surface properties of these two $ZnIn_2S_4$ polymorphs was carried out. The results reveal that hexagonal $ZnIn_2S_4$ microspheres are composed of nanolamella petals growing in the *ab* plane, ie, the negative (0001) S plane. This negative (0001) S plane not only is favorable for the adsorption of the cationic dye RhB via —$N(Et)_2$ groups, but also can accumulate the photogenerated holes, making the hole-directed photocatalytic deethylation of RhB expedient. This negative (0001) S plane of hexagonal $ZnIn_2S_4$ microspheres also show promoting effect for the degradation of cationic dye like MB, but not for the degradation of anionic dye like MO.

## 2. EXPERIMENTAL SECTION

**2.1. Preparations.** Different $ZnIn_2S_4$ polymorphs were synthesized via a hydrothermal process according to our previous report.[20] For cubic $ZnIn_2S_4$, $Zn(NO_3)_2{\cdot}6H_2O$ (0.297 g, 1 mmol), $In(NO_3)_3{\cdot}4.5H_2O$ (0.762 g, 2 mmol), and thioacetamide (TAA, 0.15 g, 2 mmol) were dissolved in 70 mL of deionized water and transferred to a 100 mL Teflon linear. The Teflon linear was sealed in the stainless steel autoclave and heated at 120 °C. After the reaction, the autoclave was cooled to room temperature. The product collected was washed with deionized water several times before it was dried at 60 °C to obtain the final product. A similar procedure was applied in the preparation of hexagonal $ZnIn_2S_4$ microspheres except that $ZnCl_2$ and $InCl_3{\cdot}4H_2O$ were used as the metal precursors.

**2.2. Characterizations.** The Brunauer–Emmett–Teller (BET) surface area was measured with an ASAP2020 M apparatus (Micromeritics Instrument Corp.). After the samples were degassed in vacuum at 120 °C until the pressure lower than $10^{-6}$ Torr, the nitrogen adsorption and desorption isotherms were measured at −196 °C. The transmission electron microscopy (TEM) and high resolution transmission electron microscopy (HRTEM) images were measured by JEOL model JEM 2010 EX instrument at the accelerating voltage of 200 kV. The powder particles were supported on a carbon film coated on a 3 mm diameter fine-mesh copper grid. A suspension in ethanol was sonicated and a drop was dripped on the support film. The Mott–Schottky curves were measured using a ZENNIUM electrochemical analyzer (Zahner, Germany) in a three-electrode cell. Pt plate and Ag/AgCl electrode (3 M KCl) were used as the counter and reference electrode, respectively. The electrolyte was a 0.2 M aqueous solution of $Na_2SO_4$. The potential ranged from −0.3 to 0.8 V (vs Ag/AgCl), while the perturbation signal was set at 20 mV with the frequency ranging from 500 to 1500 Hz. X-ray photoelectron spectroscopy (XPS) measurements were performed on a PHI Quantum 2000 XPS system (PHI, USA) with a monochromatic Al $K_\alpha$ source and a charge neutralizer. All the binding energies were referenced to the C1s peak at 284.6 eV of the surface adventitious carbon.

**2.3. Adsorption and Photocatalytic Degradation of Dyes.** The adsorption capabilities of both $ZnIn_2S_4$ polymorphs were evaluated by their adsorptions toward two cationic dyes, rhodamine B (RhB) and methylene blue (MB), and one anionic dye, mordant yellow 10 (MY10). The molecular formula of RhB, MB, MY10 are shown in the Supporting Information (Figure S1). The initial concentration of RhB, MB and MY10 were 10, 10, and 20 ppm respectively. The amount of the photocatalyst used was 5, 10, and 40 mg respectively. Aqueous solution of the dye (80 mL) and the desired amount of photocatalyst was placed in a 100 mL Pyrex vessel. The dispersion was magnetically stirred in the dark for several hours to achieve the adsorption/desorption equilibrium between the dye and the photocatalyst. The amount of the dye adsorbed was calculated using the equation $Q = ((C_0 - C)V/M)/W$, where $Q$ is the amount of dye adsorbed, $C_0$ is the initial concentration of the dye, $C$ is the concentration of the dye at adsorption/desorption equilibrium, $V$ is the solution volume, $M$ is the molecular mass of dye and $W$ is the amount of the photocatalyst used.

The photocatalytic activity of both $ZnIn_2S_4$ polymorphs was evaluated by the decomposition of RhB and MB in an aqueous solution under visible light irradiations. A 500 W tungsten halogen lamp was positioned inside a cylindrical Pyrex vessel and surrounded by a circulating water jacket (Pyrex) to cool the lamp. A cutoff filter was placed outside the Pyrex jacket to completely remove all wavelengths less than 420 nm to ensure the irradiations with visible light only. Prior to irradiations, the suspension was magnetically stirred in the dark for several hours to ensure the establishment of an adsorption/desorption equilibrium. At given irradiation time intervals, 3 mL of the suspension was collected, centrifuged, and filtered to separate the photocatalyst particles. The filtrate was analyzed by a Varian Cary 500 Scan UV–vis spectrophotometer and the absorption peaks at maximum absorption wavelength for dyes were monitored. The percentage of the degradation is reported as $A/A_0$, where $A$ is the absorption of dye at each irradiated time interval of the maximum peak of the absorption spectrum and $A_0$ is the absorption of the dye when adsorption/desorption equilibrium was achieved.

## 3. RESULTS AND DISCUSSION

Our previous study showed that cubic $ZnIn_2S_4$ nanoparticles exhibit higher photocatalytic activity for the degradation of MO than hexagonal $ZnIn_2S_4$ microspheres (see the Supporting Information, Figure S2).[20] However, when these two $ZnIn_2S_4$ polymorphs were used in the photocatalytic degradation of RhB, an opposite order was obtained. The RhB concentration change as monitored by the maximum absorption of RhB at 554 nm during the photocatalytic degradation in the presence

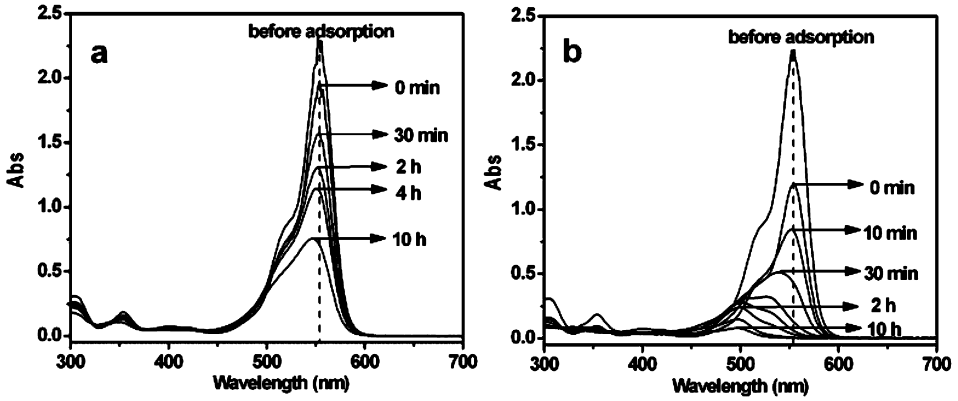


**Figure 2.** Temporal UV−vis absorption spectral changes during the photocatalytic degradation of RhB (20 ppm, 80 mL) in aqueous (a) cubic and (b) hexagonal $ZnIn_2S_4$ suspensions (0.125 g/L).

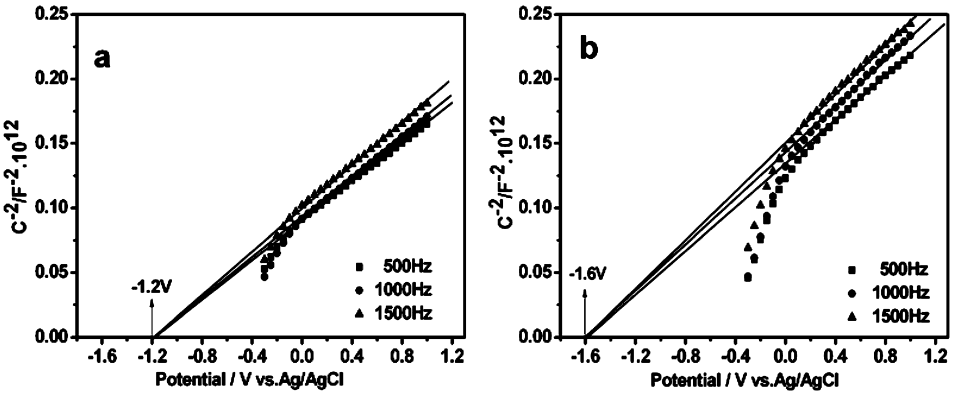


**Figure 3.** Mott−Schottky plots for (a) hexagonal and (b) cubic $ZnIn_2S_4$. The ac amplitude is 20 mV and the frequency is in the range 500−1500 Hz.

of hexagonal $ZnIn_2S_4$ microspheres and cubic $ZnIn_2S_4$ nanoparticles reveals that the degradation rate of RhB over hexagonal $ZnIn_2S_4$ microspheres is greater than that over the cubic one (Figure 1a). An almost complete conversion of RhB occurred within 2 h in irradiated hexagonal $ZnIn_2S_4$ microspheres dispersions. On the contrary, only about 63% of RhB was converted after irradiated for 10 h in the presence of cubic $ZnIn_2S_4$ nanoparticles. Only 5% of RhB was decomposed in 10 h under pure visible light irradiations, indicating that the decomposition of RhB over both $ZnIn_2S_4$ polymorphs is mainly induced by photocatalysis. The degradation of RhB follows a fairly good correlation to the pseudofirst-order reaction kinetics for both $ZnIn_2S_4$ systems and the determined reaction rate constant $k$ for RhB degradation is 1.66 and 0.12 $h^{-1}$ for hexagonal and cubic $ZnIn_2S_4$ respectively (Figure 1b). Therefore, the photocatalytic activity for the degradation of RhB is higher over hexagonal $ZnIn_2S_4$ microspheres, which is opposite to what we have observed previously in the degradation of MO. Another noticeable difference between these two $ZnIn_2S_4$ polymorphs is that the spectral changes during the photocatalytic degradation of RhB are quite different. The temporal UV−vis spectral changes of RhB solution during the photocatalytic degradation reactions over two $ZnIn_2S_4$ polymorphs reveals that the extent of the hypsochromic shift in the presence of hexagonal $ZnIn_2S_4$ microspheres is much larger than that in the cubic $ZnIn_2S_4$ nanoparticles (Figure 2). The main absorbance of RhB solution shifts gradually from the initial 554 to 498 nm, a total 56 nm hypsochromic shift in 2 h, in the presence of hexagonal $ZnIn_2S_4$ microspheres. However, only a negligible blue shift (2 nm) is observed within a similar reaction time in the presence of cubic $ZnIn_2S_4$ dispersion (Figure 2). Because the gradual hypsochromic shift in the maximum absorbance of RhB has been well proved to be derived from a step-by-step de-ethylation of RhB, whereas the decrease in the characteristic band can be due to the destruction of the chromophore structure in RhB, the marked hypsochromic shift over hexagonal $ZnIn_2S_4$ system indicates a much faster de-ethylation process over hexagonal $ZnIn_2S_4$ microspheres as compared to that over cubic $ZnIn_2S_4$ nanoparticles.[23] Therefore, it is clear that a preferential N-deethylation process occurs before the destruction of the chromophore structure in the hexagonal $ZnIn_2S_4$ system, while a direct cleavage of the RhB chromophore process predominates in the cubic $ZnIn_2S_4$ system.

It is interesting to observe that hexagonal $ZnIn_2S_4$ microspheres and cubic $ZnIn_2S_4$ nanoparticles exhibit different pathways in the degradation of RhB and these two $ZnIn_2S_4$ show an opposite photocatalytic activity order in the degradation of RhB and MO. Since the photocatalytic performance of a photocatalyst is strongly related to factors like crystallinity, band structure, specific surface area, and surface properties, a detailed study of the physicochemical properties of these two $ZnIn_2S_4$ polymorphs have been carried out to elucidate the different photocatalytic performance over these two $ZnIn_2S_4$ polymorphs. Considering that both $ZnIn_2S_4$ polymorphs are well crystallized and have comparable band gap (2.5 for hexagonal and 2.3 eV for cubic $ZnIn_2S_4$ respectively), the crystallinity and the optical absorption should not have

opposite effect in the degradation of different model compounds (RhB and MO) (see the Supporting Information, Figures S3 and S4). Therefore the influence played by the crystallinity and the optical absorption of two $ZnIn_2S_4$ polymorphs should be excluded. The band position is another important factor in influencing the performance of a photocatalyst since they influence the redox ability of the photogenerated charge carriers. To determine the band position of these two $ZnIn_2S_4$ polymorphs, Mott−Schottky (M-S) plots of these materials were measured at frequency of 500, 1000, and 1500 Hz and the ac amplitude was set at 20 mV. As shown in Figure 3, the intersection points do not depend on the different frequency applied and the flat band positions determined from the intersection are approximately −1.2 and −1.6 V versus Ag/AgCl (−1.0 V and −1.4 V vs NHE) for hexagonal and cubic phase, respectively. Since it is generally believed that the bottom of the conduction band in many *n*-type semiconductors is more negative by ∼-0.1 V than the flat band potential,[24,25] the conduction band can be estimated to be −1.1 and −1.5 V vs NHE, whereas the valence band can be calculated to be 0.9 and 1.5 V vs NHE for cubic and hexagonal $ZnIn_2S_4$, respectively (Scheme 1). It is found that the valence band of both $ZnIn_2S_4$

**Scheme 1. Calculated Band Positions of Hexagonal and Cubic $ZnIn_2S_4$ Polymorphs, and Possible Mechanism of the Visible-Light-Driven Photocatalysis over Different $ZnIn_2S_4$ Polymorphs**

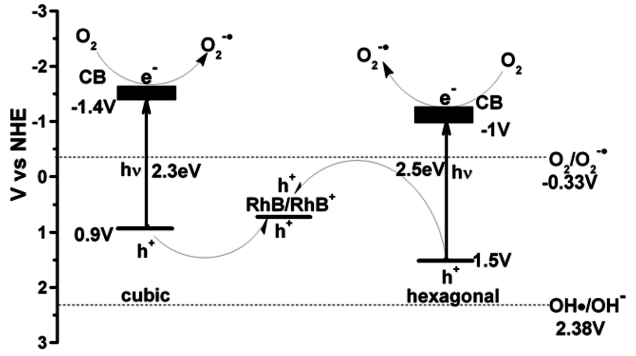


polymorphs is less positive than that of $E°$ (•OH/$OH^-$) (2.38 V vs NHE), therefore the photogenerated holes are not able to oxidize $OH^-$ to give •OH. However, the conduction band of both $ZnIn_2S_4$ polymorphs are negative than that of $E°(O_2/O_2^-•)$ (−0.33 V vs NHE), indicating that the photogenerated electrons can reduce the surface chemisorbed $O_2$ to yield the strong oxidizing species $O_2^-•$. The decomposition of the chromophores in RhB or a deeper oxidation of the reaction intermediates to small molecules like $CO_2$ during the photocatalytic degradation of RhB are believed to be brought about by these $O_2^-•$ species.[26,27] The capability of generating $O_2^-•$ species over both $ZnIn_2S_4$ polymorphs can rationalize the occurrence of a total decomposition of RhB over these $ZnIn_2S_4$ polymorphs. However, since the photocatalytic de-ethylation of RhB is attributed to the photogenerated holes, and the holes generated over both $ZnIn_2S_4$ polymorphs can directly oxidize RhB (Scheme 1), why these two $ZnIn_2S_4$ polymorphs exhibit different pathways and why hexagonal $ZnIn_2S_4$ microspheres show a higher activity than the cubic one in the degradation of RhB can not be interpreted in terms of their different band positions.

As we know, a prerequisite for a direct hole-oxidation of RhB leading to the de-ethylated intermediates is the adsorption of RhB on the photocatalyst surface via —$N(Et)_2$ groups.[28] The much higher de-ethylation rate over hexagonal $ZnIn_2S_4$ microspheres than cubic $ZnIn_2S_4$ nanoparticles implies that hexagonal $ZnIn_2S_4$ microspheres must have higher adsorption capability toward RhB than the cubic one and RhB is adsorbed on the surface via —$N(Et)_2$ groups.[23,27,28] This assumption is confirmed by both the adsorption experiments and the XPS results. The adsorption experiments reveal that hexagonal $ZnIn_2S_4$ microspheres exhibit a higher adsorption capability toward RhB as compared to cubic $ZnIn_2S_4$ nanoparticles. As shown in Figure 2, for RhB solution with an initial concentration of 10 ppm, 46.1% RhB was adsorbed over 5 mg of hexagonal $ZnIn_2S_4$ microspheres dispersion, whereas only 11.2% RhB was adsorbed over cubic $ZnIn_2S_4$ dispersion. The adsorption capability toward RhB was calculated to be 154.3 and 37.4 $\mu$mol/g over hexagonal and cubic $ZnIn_2S_4$ respectively (Figure 4). The higher adsorption toward RhB

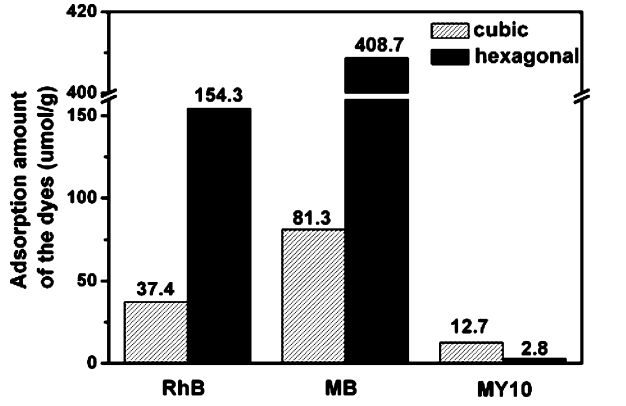


**Figure 4.** Adsorption amounts of various kinds of dyes over hexagonal and cubic $ZnIn_2S_4$ samples.

over hexagonal $ZnIn_2S_4$ microspheres as compared to cubic polymorph can not be induced by its higher BET specific surface area since the determined BET surface area is 65.64 $m^2$ $g^{-1}$ for the hexagonal microspheres, less than that for the cubic one (93.86 $m^2$ $g^{-1}$) (Figure 5). Generally, the pH values of suspension may influence the adsorption and activity of catalysts. However, the pH values were equivalent for both two systems. Therefore, the influences of pH values were eliminated for adsorption. The XPS result also confirms the assumption that RhB is adsorbed on the surface of hexagonal $ZnIn_2S_4$ microspheres via —$N(Et)_2$ groups. The XPS spectrum in the N 1s region of RhB adsorbed hexagonal $ZnIn_2S_4$ microspheres show two obvious peaks at 399.2 and 400.3 eV (Figure 6a). The peak at 399.2 eV can be assigned to free —$N(Et)_2$ groups of RhB without interactions with the photocatalyst surface, whereas the peak at 400.3 eV can be assigned to —$N(Et)_2$ groups of RhB binding to the $S^{2-}$ sites on the photocatalyst surface.[27] On the contrary, the XPS in the N 1s region of RhB adsorbed on cubic $ZnIn_2S_4$ nanoparticles only show one obvious peak located at 399.3 eV (Figure 6b), which can be assigned to free —$N(Et)_2$ groups of RhB without interactions with the photocatalyst surface. The different adsorption modes and adsorption capabilities toward RhB observed over these two $ZnIn_2S_4$ polymorphs may be related to their different surface characteristics.

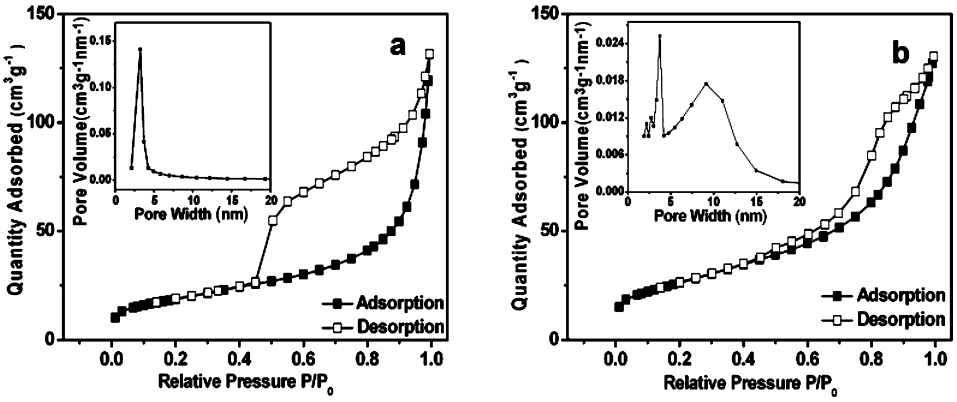


**Figure 5.** Nitrogen adsorption−desorption isotherms of (a) hexagonal and (b) cubic $ZnIn_2S_4$. Inset: Pore size distribution curve of the as-prepared samples calculated from desorption branch of the nitrogen isotherm by the BJH method.

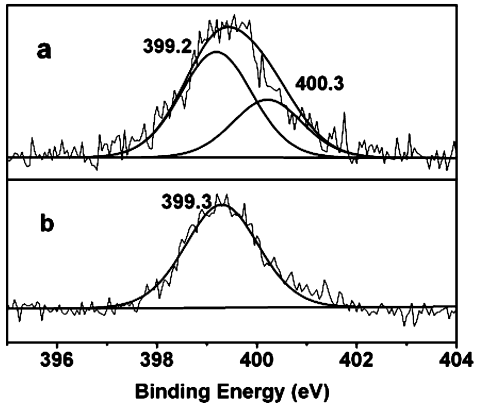


**Figure 6.** XPS spectra in N 1s region for RhB adsorbed on (a) hexagonal $ZnIn_2S_4$ and (b) cubic $ZnIn_2S_4$.

The preferential adsorption toward RhB and the adsorption via $—N(Et)_2$ groups implies that hexagonal $ZnIn_2S_4$ microspheres may possess more surface anionic sites for the adsorption than cubic $ZnIn_2S_4$ nanoparticles. Usually, the increase in the surface anionic sites could be attributed to the surface modifications or the presence of the specific surface crystal facet.[27,29] For example, previous studies revealed that the modifications of $TiO_2$ or $In(OH)_yS_z$ solid solution with $F^-$ ions may increase their adsorption capability toward the cationic dye like RhB.[27,28] In our case, we believe that the presence of the specific surface crystal facet may take the responsibility in increasing the surface anionic sites since hexagonal $ZnIn_2S_4$ microspheres are composed of numerous densely packed petals, indicating of anisotropy.

TEM and HRTEM images of the hexagonal $ZnIn_2S_4$ microspheres with nanolamella petals are shown in Figure 7a and 7b. HRTEM image of a petal from hexagonal $ZnIn_2S_4$ microsphere exhibits a hexagonal lattice with the interlayer distance of 0.33 nm, which corresponds to the (100) spacing of hexagonal $ZnIn_2S_4$. The fast Fourier transform (FFT) pattern is consistence with the diffraction pattern of the [0001] zone axis of hexagonal $ZnIn_2S_4$ (inset in Figure 7b). Therefore HRTEM and the corresponding FFT indicate that the hexagonal $ZnIn_2S_4$ petal grows in the *ab* plane, perpendicular to the [0001] axis. The crystal structure of hexagonal $ZnIn_2S_4$ with the projection along *c* axis is shown in Figure 7c. In hexagonal $ZnIn_2S_4$, the stacking of atoms is in a repeated sequence of S−Zn−S−In−S−In−S along the *c* axis. Apparently the (0001) *ab* plane contains exclusively of sulfur atoms and is negative. This negatively charged S (0001) plane would have stronger interaction with positively charged RhB molecules via $—N(Et)_2$ groups. This may account for a higher adsorption capability toward RhB over the hexagonal $ZnIn_2S_4$ microspheres as compared to cubic $ZnIn_2S_4$ sample, which is composed of nanoparticles.

To validate the above assumption that hexagonal $ZnIn_2S_4$ microspheres composed of nanolamella petals with (0001) negatively charged S plane would preferentially adsorb cationic dyes, another cationic dye, methylene blue (MB), and another anionic dye, mordant yellow 10 (MY10), were chosen as the model target dyes and the adsorption capabilities of two $ZnIn_2S_4$ polymorphs toward two dyes were shown in Figure 4.

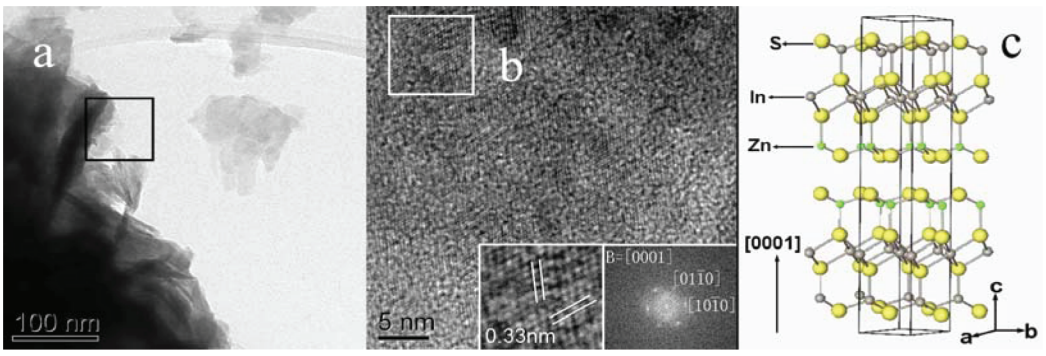


**Figure 7.** (a) TEM and (b) HRTEM images and (c) illustration of crystal structure of hexagonal $ZnIn_2S_4$. The inset of b is the FFT pattern.


dx.doi.org/10.1021/am300272f | ACS Appl. Mater. Interfaces 2012, 4, 2273−2279

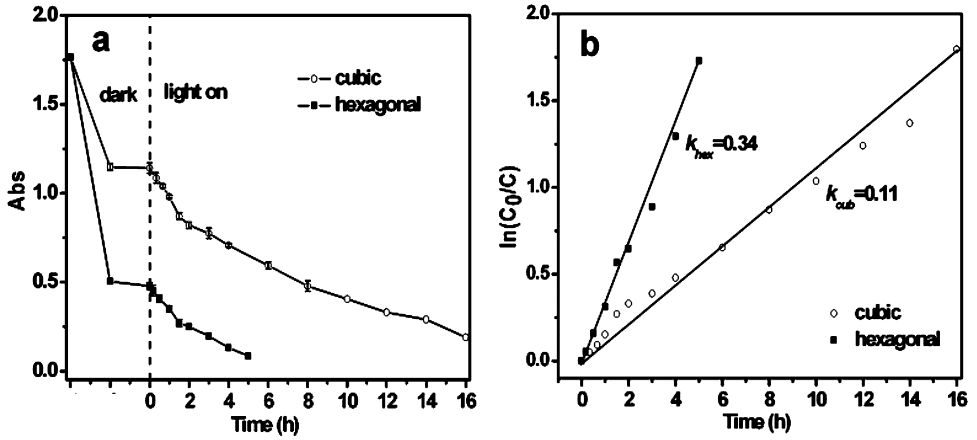


**Figure 8.** (a) Temporal course of photocatalytic degradation, and (b) pseudofirst-order plots comparing photocatalytic of degradation MB (10 ppm, 80 mL) in aqueous dispersions containing 10 mg of catalysts, where $k_{cub}$ and $k_{hex}$ are the first-order rate constant of cubic and hexagonal $ZnIn_2S_4$, respectively.

As expected, hexagonal $ZnIn_2S_4$ microspheres show much higher adsorption capability toward cationic dye than cubic $ZnIn_2S_4$ nanoparticles. The adsorption capability toward MB is 408.7 and 81.3 $\mu$mol/g over hexagonal and cubic $ZnIn_2S_4$ respectively. On the contrary, cubic $ZnIn_2S_4$ nanoparticles show higher adsorption capability toward anionic dye MY10 (12.7 $\mu$mol/g for cubic $ZnIn_2S_4$ vs 2.8 $\mu$mol/g for hexagonal $ZnIn_2S_4$) (Figure 4).

The (0001) negatively charged S plane on hexagonal $ZnIn_2S_4$ microspheres not only can enhance the adsorption toward cationic dyes, but also can selectively accumulate the photogenerated holes. Hexagonal $ZnIn_2S_4$ has a layer structure consists of different atom layers arranged in a repeated sequence of S−Zn−S−In−S−In−S along the *c* axis (Figure 7c). Previous literature has revealed that the S3p orbitals make a significant contribution to the valence band top of hexagonal $ZnIn_2S_4$.[30] Therefore the photogenerated holes would locate in the sulfur layer when hexagonal $ZnIn_2S_4$ is photoexcited. If the photogenerated holes can directly oxidize the dye molecules, the accumulation of the holes and the high adsorption of cationic dyes over this (0001) negatively charged S plane would make the hole-directed photocatalytic activity extremely high over the hexagonal $ZnIn_2S_4$ microspheres. Similar to the deethylation of RhB, the demethylation of MB, has also been observed to be faster over hexagonal $ZnIn_2S_4$ microspheres than over cubic $ZnIn_2S_4$ nanoparticles. A complete demethylation of MB occurred in 5 h over hexagonal $ZnIn_2S_4$ microspheres, while only about 46% of MB was degraded over cubic $ZnIn_2S_4$ nanoparticles (Figure 8). However, for MO, an anionic dye, because the photogenerated holes can not directly oxidize MO, the photocatalytic activity order is opposite over these two $ZnIn_2S_4$ polymorphs. The degradation of MO is mainly a reduced process, which attributed to the photogenerated electrons. Therefor, the $S^{2-}$ of $ZnIn_2S_4$ tend to be oxidized by the remained photogenerated hole led to photocorrosion occur during the degradation of MO, which different from degradation of RhB and MB. Because of a more negative conduction band and a high optical absorption, cubic $ZnIn_2S_4$ nanoparticles show a better photocatalytic activity for MO degradation as compared to hexagonal $ZnIn_2S_4$ microspheres.

## 4. CONCLUSIONS

Hexagonal $ZnIn_2S_4$ microspheres exhibit a different pathway and a higher photocatalytic activity in the degradation of RhB as compared to cubic $ZnIn_2S_4$ nanoparticles. These phenomena can be well explained in terms of the exposed negative (0001) S plane which comprises the hexagonal $ZnIn_2S_4$ microspheres. The negative (0001) S plane, which can not only enhance the adsorption of cationic dyes over hexagonal $ZnIn_2S_4$ microspheres but also accumulate the photogenerated holes, making the hole-direct photocatalytic degradation of cationic dyes extremely high over the hexagonal $ZnIn_2S_4$ microspheres. Our results provide some new insights in how the surface facet can take effect on influencing the performance of a photocatalyst and why different polymorphs can exhibit different photocatalytic performances. The results can also provide some guidance in the development of new efficient photocatalysts.

## ■ ASSOCIATED CONTENT

### Supporting Information

Molecular formulas of rhodamine B (RhB), methyl orange (MO), methylene blue (MB), and mordant yellow 10 (MY10); photocatalytic degradation of MO; XRD and UV-DRS spectra of both $ZnIn_2S_4$ polymorphs. This material is available free of charge via the Internet at http://pubs.acs.org/.

## ■ AUTHOR INFORMATION

### Corresponding Author

*E-mail: zhaohuili1969@yahoo.com. Tel: 86-591-83779260.

### Notes

The authors declare no competing financial interest.

## ■ ACKNOWLEDGMENTS

The work was supported by National Natural Science Foundation of China (20977016 and U1033603), National Basic Research Program of China (973 Program: 2011CB612314) and Program for Changjiang Scholars and Innovative Research Team in University (PCSIRT0818). The Award Program for Minjiang Scholar Professorship and the NSF of Fujian province for Distinguished Young Investigator Grant (2009J06004) to Z.L. are also acknowledged.

## REFERENCES


(1) Hoffmann, M. R.; Martin, S. T.; Choi, W.; Bahnemann, D. W. *Chem. Rev.* **1995**, *95*, 69−96.
(2) Fujishima, A.; Rao, T. N.; Tryk, D. A. *J. Photochem. Photobiol. C* **2000**, *1*, 1−21.
(3) Chen, C. C.; Ma, W. H.; Zhao, J. C. *Chem. Soc. Rev.* **2010**, *39*, 4206−4219.
(4) Ouyang, S. X.; Ye, J. H. *J. Am. Chem. Soc.* **2011**, *133*, 7757−7763.
(5) He, D.; Wang, L.; Xu, D.; Zhai, J.; Wang, D.; Xie, T. *ACS Appl. Mater. Interfaces* **2011**, *3*, 3167−3171.
(6) Yu, J. G.; Dai, G. P.; Huang, B. B. *J. Phys. Chem. C* **2009**, *113*, 16394−16401.
(7) Zhou, W.; Liu, H.; Wang, J.; Liu, D.; Du, G.; Cui, J. *ACS Appl. Mater. Interfaces* **2010**, *2*, 2385−2392.
(8) Zhu, S.; Xu, T.; Fu, H.; Zhao, J.; Zhu, Y. *Environ. Sci. Technol.* **2007**, *41*, 6234−6239.
(9) Zhang, L.; Yin, L.; Wang, C.; Lun, N.; Qi, Y. *ACS Appl. Mater. Interfaces* **2010**, *2*, 1769−1773.
(10) Dong, H.; Li, Z.; Xu, X.; Ding, Z.; Wu, L.; Wang, X.; Fu, X. *Appl. Catal. B: Environ.* **2009**, *89*, 551−556.
(11) Sriram, M. A.; McMichael, P. H.; Waghray, A.; Kumta, P. N.; Misture, S.; Wang, X. L. *J. Mater. Sci.* **1998**, *33*, 4333−4339.
(12) Georgobiani, A. N.; Iyuknina, Z. P.; Tiginyanu, I. M. *Sov. Phys. Semicond.* **1982**, *16*, 231−232.
(13) Romeo, N.; Dallaturca, A.; Braglia, R.; Sberveglieri, G. *Appl. Phys. Lett.* **1973**, *2*, 21−22.
(14) Seo, W. S.; Otsuka, R.; Okuno, H.; Ohta, M.; Koumoto, K. *J. Mater. Res.* **1999**, *14*, 4176−4181.
(15) Shen, S. H.; Zhao, L.; Guo, L. J. *Int. J. Hydrogen Energy* **2008**, *33*, 4501−4510.
(16) Lei, Z. B.; You, W. S.; Liu, M. Y.; Zhou, G. H.; Takata, T.; Hara, M.; Domen, K.; Li, C. *Chem. Commun.* **2003**, 2142−2143.
(17) Hu, X. L.; Yu, J. C.; Gong, J. M.; Li, Q. *Cryst. Growth Des.* **2007**, *7*, 2444−2448.
(18) Chen, Z. X.; Li, D. Z.; Zhang, W. J.; Shao, Y.; Chen, T. W.; Sun, M.; Fu, X. Z. *J. Phys. Chem. C* **2009**, *113*, 4433−4440.
(19) Fang, F.; Chen, L.; Chen, Y. B.; Wu, L. M. *J. Phys. Chem. C* **2010**, *114*, 2393−2397.
(20) Chen, Y. J.; Hu, S. W.; Liu, W. J.; Chen, X. Y.; Wu, L.; Wang, X. X.; Liu, P.; Li, Z. H. *Dalton Trans.* **2011**, *40*, 2607−2613.
(21) Yang, H.; Sun, C.; Qiao, S.; Zou, J.; Liu, G.; Smith, S.; Cheng, H.; Lu, G. *Nature* **2008**, *453*, 638−641.
(22) Zhou, K.; Li, Y. *Angew. Chem., Int. Ed.* **2012**, *51*, 602−613.
(23) Chen, C. C.; Zhao, W.; Zhao, J. C. *Chem.—Eur. J.* **2004**, *10*, 1956−1963.
(24) Matsumoto, Y. *J. Solid State Chem.* **1996**, *126*, 227−237.
(25) Matsumoto, Y.; Omae, K.; Watanabe, I.; Sato, E. *J. Electrochem. Soc.* **1986**, *133*, 711−716.
(26) Li, Z. H.; Dong, H.; Zhang, Y. F.; Dong, T. T.; Wang, X. X.; Li, J. Q.; Fu, X. Z. *J. Phys. Chem. C* **2008**, *112*, 16046−16051.
(27) Hu, S. W.; Zhu, J.; Wu, L.; Wang, X. X.; Liu, P.; Zhang, Y. F.; Li, Z. H. *J. Phys. Chem. C* **2011**, *115*, 460−467.
(28) Wang, Q.; Chen, C. C.; Zhao, D.; Ma, W. H.; Zhao, J. C. *Langmuir* **2008**, *24*, 7338−7345.
(29) Li, Q. Y.; Kako, T.; Ye, J. H. *Appl. Catal., A* **2010**, *375*, 85−91.
(30) Shen, S. H.; Zhao, L.; Zhou, Z. H.; Guo, L. J. *J. Phys. Chem. C* **2008**, *112*, 16148−16155.